CORE
Metadata, citation and similar papers at core.ac.uk
Provided by Arrow@dit

Technological University Dublin
ARROW@TU Dublin

Articles

Biomedical Devices and Assistive Technology Research Group

2010-03-10

A Linear Finite Element Acoustic Fluid-Structure Model of Ultrasonic Angioplasty in Vivo

Mark Wylie
Technological University Dublin, mark.wylie@tudublin.ie

Garrett McGuinness
Dublin City University, garrett.mcguinness@dcu.ie

Graham Gavin
Technological University Dublin, graham.gavin@tudublin.ie

Follow this and additional works at: https://arrow.tudublin.ie/biodevart

 Part of the Biomedical Engineering and Bioengineering Commons

Recommended Citation
Wylie, M., McGuinness, G., Graham, G. (2010) A Linear Finite element Acoustic Fluid-Structure Model of Ultrasonic Angioplasty in Vivo. *International Journal for Numerical Methods in Biomedical Engineering.* vol.26, no.7,pp.828–842. doi:10.1002/cnm.1383

This Article is brought to you for free and open access by the Biomedical Devices and Assistive Technology Research Group at ARROW@TU Dublin. It has been accepted for inclusion in Articles by an authorized administrator of ARROW@TU Dublin. For more information, please contact yvonne.desmond@tudublin.ie, arrow.admin@tudublin.ie, brian.widdis@tudublin.ie.

This work is licensed under a Creative Commons Attribution-Noncommercial-Share Alike 3.0 License

A LINEAR FINITE ELEMENT ACOUSTIC FLUID-STRUCTURE MODEL OF ULTRASONIC ANGIOPLASTY *IN VIVO*

Mark P. Wylie[1, 3], Garrett B. McGuinness[2] and Graham P. Gavin[1, 3*]

[1]School of Manufacturing and Design Engineering, Dublin Institute of Technology, Ireland.
[2]School of Mechanical and Manufacturing Engineering, Dublin City University, Ireland.
[3]Biomedical Devices and Assistive Technologies Research Group, Dublin Institute of Technology, Ireland.

* Corresponding author

Abstract

The delivery of high-power ultrasonic energy via small diameter wire waveguides represents a new alternative therapy for the treatment of chronic totally occluded arteries (CTOs). This type of energy manifests itself as a mechanical vibration at the distal-tip of the waveguide with amplitudes of vibration up to 60 µm and at frequencies of 20- 50 kHz. Disruption of diseased tissue is reported to be a result of direct mechanical ablation, cavitation, pressure components and acoustic streaming and that ablation was only evident above the cavitation threshold. This work presents a linear finite element acoustic fluid-structure model of an ultrasonic angioplasty waveguide *in vivo*. The model was first verified against a reported analytical solution for an oscillating sphere. It was determined that 140 elements per wavelength (EPW) were required to predict the pressure profile generated by the wire waveguide distal-tip. Implementing this EPW count, the pressure field surrounding a range of distal-tip geometries was modelled. For validation, a model was developed with parameters based on a bench-top experiment from the literature of an ultrasonic wire waveguide in a phantom leg. This model showed good correlation with the experimental measurements. These models may aid in the further development of this technology.

Key Words: *Finite element analysis, ultrasound, angioplasty, acoustic, cavitation.*

NOMENCLATURE

$\boldsymbol{P_{max}}$ = *Pressure amplitude at a location in the fluid, see Figure 2.*

$\boldsymbol{d}$ = *amplitude of vibration of the sphere.*

$\boldsymbol{f}$ = *frequency of vibration of the sphere.*

$\boldsymbol{R}$ = *radius of the sphere.*

$\boldsymbol{\rho}$ = *fluid density.*

$\boldsymbol{r}$ = *radial distance from centre of sphere.*

$\boldsymbol{\theta}$ = *angle between the direction of oscillation and radius-vector, see Figure 2.*

$\boldsymbol{\alpha_r}$ = *sound power reflection coefficient.*

$\boldsymbol{c}$ = *speed of sound in fluid.*

$\boldsymbol{k}$ = *bulk modulus of fluid.*

$(\ddot{\vec{P}})$ = *the 2nd derivative of the nodal pressure vector.*

$(\vec{P})$ = *the nodal pressure vector.*

$(\ddot{\vec{u}})$ = *the 2nd derivative of the nodal displacement vector.*

$(\vec{u})$ = *the nodal displacement vector.*

$[M_F]$ = *Fluid mass matrix.*

$[K_F]$ = *Fluid stiffness matrix.*

$[M_S]$ = *Structure mass matrix.*

$[K_S]$ = *Structure stiffness matrix.*

[R] = a coupling matrix that represents effective surface area associated with each node on the fluid structure interface.

$(\vec{F}_s)$ = *the fluid pressure load vector.*

1. INTRODUCTION

a. Clinical Background

The majority of atherosclerotic lesions can be treated by percutaneous interventional dilation procedures such as balloon angioplasty and stent implantation. These procedures require that the partial blockage must first be accessed by a guidewire, a small diameter wire that ensures that the plaque can be crossed (a key indicator of success) and also acts as a guiderail for the balloon and stent delivery systems. Lesions resulting in a near or totally blocked artery, known as chronic total occlusions (CTOs) pose a significant challenge to standard dilation procedures and may represent up to 16% of all coronary plaques [1].

Advanced stages of CTOs are often accompanied by significant fibrous material and calcification which can also hinder successful dilation procedures and optimal stent implantation. In many cases involving CTOs, fully invasive surgery is often the only available option and in recent years this has provided an impetus to develop alternative minimally invasive techniques for these challenging chronic total occlusions.

A new minimally invasive approach to near or totally occluded plaques involves the use of low-frequency ultrasonic longitudinal waves transmitted through a wire waveguide. In 2007 this technology was approved for use in both the United States and Europe [2]. The ultrasound energy establishes a longitudinal mechanical standing wave in the wire waveguide with the frequency and amplitude being determined by the output power of the external transducer and acoustic horn as shown in Figure 1. Using this configuration, frequencies in the region of 20-50 kHz and amplitudes of vibration at the waveguide distal-tip of up to 60 µm are commonly reported. At the distal-tip of the waveguide, tissue is thought to be disrupted by a number of mechanisms; primarily direct mechanical ablation and cavitation, and to a lesser extent acoustic streaming and pressure wave components [3]. It has been reported that this method of tissue disruption has the advantage of selective tissue removal. At the right combination of frequency and amplitude it can disrupt rigid diseased tissue while healthy elastic tissue remains largely unaffected [4].

Acoustic pressures developed at the waveguide-fluid/tissue interface appear to play a significant role with some authors observing that plaque ablation was only evident above the cavitation threshold [4]. As a result, frequencies are typically kept below 50 kHz for the reason that the intensity and power required to produce cavitation greatly increase above frequencies of 100 kHz [5]. It has been suggested that a rough distal-tip encourages the onset of cavitation by introducing trapped gas nuclei into the fluid. Microbubble agents may also be artificially introduced to the volume surrounding the vibrating waveguide distal-tip to lower the cavitation threshold. Enlarged distal-tips are commonly utilised to enhance cavitation, reduce events of arterial perforation of the surrounding healthy arterial wall and generate larger post-operative lumens for follow up devices.

b. Acoustic Pressure

The significance of the pressure amplitude at the waveguide distal-tip, the subsequent cavitation and pressures developed in surrounding fluids and tissues has led a number of researchers to investigate this phenomenon. Analytical solutions of simplified geometries and conditions exist, namely the solution for a pulsating sphere in a fluid and the more representative oscillating sphere in a fluid. The Morse solution [6] for the pressure field near an oscillating sphere in a fluid is given in Equation 1. Figure 2 illustrates the parameters appearing in this solution. Although this linear solution is limited to a simple geometry, it has been suggested by Nyborg [7] as a useful approximation to predict pressure amplitudes and subsequent cavitation associated with the frequencies and conditions encountered in ultrasound angioplasty.

$$P_{\max} = 2\pi^2 \rho R f^2 d \times \frac{R^2 |\cos\theta|}{r^2} \qquad \text{(Equation 1)}$$

where: P_{max} = *Pressure amplitude at a location in the fluid, a function of* θ *and r*
d = *amplitude of vibration of the sphere*
f = *frequency of vibration of the sphere*
R = *radius of the sphere*
ρ = *fluid density*
r = *radial distance from centre of sphere*
θ = *the angle between the direction of oscillation and radius-vector, see Figure 2*

While the majority of previous experimental work from the literature has focused on end clinical results some researchers have performed experimental studies on the mechanical effects of ultrasonic vibrating waveguides in simulated *in vivo* conditions [3-4, 8-9]. Experimental studies by Makin and Everbach [10] investigated the acoustic pressures developed by an ultrasonic vibrating wire waveguide submerged in a liquid with acoustic properties similar to blood. For their experiments they used both water and a glycerine-water mix. The experiment studied a wire waveguide with a 2.46 mm diameter spherical distal-tip oscillating in an acrylic cylinder filled with the fluid (representing a peripheral arterial phantom) at 22.5 kHz. Figure 3 shows a diagram of the experiment. Pressures were measured in the range of 12-250 mm (along line marked AA in Figure 3) from the vibrating distal-tip using an acoustic hydrophone; measurements in the vicinity of the distal-tip were restricted due to the limitations of their measuring equipment.

Their results demonstrate two important effects of the ultrasound *in vivo*:

i. Despite not being able to directly measure pressures at the distal-tip they were able to measure cavitation activity with a 20 MHz focused transducer. They concluded that not only was cavitation evident but that the amount of cavitation was related to the distal-tip amplitude of vibration and also to the distal-tip geometry.

ii. Their results also showed a standing wave in the acoustic domain of significant amplitude. They concluded that because the acrylic walls were acoustically transparent at the frequency used this standing wave was caused by an impedance mismatch between the liquid representative of blood and the surrounding air. This is similar to the tissue-air interface encountered in peripheral limbs *in vivo*. This standing wave is caused by reflection (wave reflections shown as dashed lines in Figure 3) that occurs at the interface of layers/materials of different acoustic impedance .The sound power reflection coefficient is given as [11]:

$$\alpha_r = \left(\frac{\rho_2 c_2 - \rho_1 c_1}{\rho_2 c_2 + \rho_1 c_1} \right)^2 \qquad \text{(Equation 2)}$$

where: α_r *= sound power reflection coefficient*
c*= speed of sound in fluid medium*

Thus assuming no energy loss, the total reflection of the incident energy must correspond to a unity value of reflection coefficient. The speed of sound for air and blood/tissue was taken as 340 m/s and 1580 m/s respectively and with densities of 1.2 kg/m^3 and 1050 kg/m^3 respectively. Using equation 2 and the material properties shown, the sound power reflection can be calculated to be 99.9% at a tissue-air interface.

c. Finite Element Modelling of Ultrasound Angioplasty

High power ultrasound in medical applications is fundamentally a non-linear propagation of sound waves above approximately 20 kHz. This derives from the non-linear pressure-density relationship and variance in speed of sound with pressure amplitude during compression/rarefaction cycle; this has a greater influence at higher frequencies and at greater intensities.

For solving finite element acoustic fluid-structure interaction models, the Navier-Stokes equations of fluid momentum and the flow continuity equation must be considered along with the structural dynamics equation. Assuming linear wave propagation, for an incompressible fluid with no mean flow, neglecting shear stresses and with mean density and pressure uniform throughout the fluid, the lossless acoustic wave equation can be written as:

$$\frac{1}{c^2}\frac{\partial^2 P}{\partial t^2} - \nabla^2 P = 0 \qquad \text{(Equation 3)}$$

where:

$$c = \sqrt{\frac{k}{\rho}} \qquad \text{(Equation 4)}$$

and: k *= bulk modulus of fluid*

The governing equation for acoustic wave propagation, given in equation 3, can be discretized taking into account the coupling of acoustic pressure and structural motion at the fluid-structure interface [12].

Fluid: $$[M_F](\ddot{\vec{P}}) + [K_F](\vec{P}) + \rho[R]^T(\ddot{\vec{u}}) = 0 \qquad \text{(Equation 5)}$$

Structural: $$[M_S](\ddot{\vec{u}}) + [K_S](\vec{u}) - [R](\vec{P}) = (\vec{F}_S) \qquad \text{(Equation 6)}$$

where:

$(\ddot{\vec{P}})$ = *the 2nd derivative of the nodal pressure vector*

$(\vec{P})$ = *the nodal pressure vector*

$(\ddot{\vec{u}})$ = *the 2nd derivative of the nodal displacement vector*

$(\vec{u})$ = *the nodal displacement vector*

$[M_F]$ = *Fluid mass matrix*

$[K_F]$ = *Fluid stiffness matrix*

$[M_S]$ = *Structure mass matrix*

$[K_S]$ = *Structure stiffness matrix*

[R] = a coupling matrix that represents effective surface area associated with each node on the fluid structure interface.

$(\vec{F}_s)$ = *the fluid pressure load vector*

The equations given in Equation 5 and 6 can be combined into a single relationship that describes load quantities at all locations in the fluid and structure as shown in Equation 7.

Combined: $$\begin{bmatrix} M_S & 0 \\ \rho_0 R^T & M_F \end{bmatrix}\begin{pmatrix} \ddot{\vec{u}} \\ \ddot{\vec{P}} \end{pmatrix} + \begin{bmatrix} K_S & -R \\ 0 & K_F \end{bmatrix}\begin{pmatrix} \vec{u} \\ \vec{P} \end{pmatrix} = \begin{pmatrix} \vec{F}_S \\ 0 \end{pmatrix} \qquad \text{(Equation 7)}$$

Finite element models of ultrasound angioplasty to date have focussed on modelling how the wire waveguide transmits the ultrasonic waves to the distal-tip. Gavin *et al* [13] performed a modal and harmonic analysis to determine wire waveguide resonant characteristics, damping and stresses. A mesh density analysis showed the importance of having an adequate mesh density to resolve the wave structure accurately. The same authors also modelled the effect the presence of fluid had on the resonant response of waveguides, concluding that the effect was negligible due to the low forces encountered at the distal-tip but that hydrodynamic effects, such as drag on the distal-tip may play a more critical role [14].

The goal of this work is to assess the finite element method as a tool to predict the acoustic conditions encountered during ultrasound angioplasty using a linear acoustic

fluid-structure model of an ultrasonic wire waveguide in simulated *in vivo* conditions (i.e. in a peripheral artery).

Initially, this includes determining adequate mesh densities for the frequency range and amplitudes of vibration of interest and comparing the results with the analytical solution outlined in equation 1. Using this verified model, the pressures near the distal-tip of the waveguide for a range of distal-tip geometries are predicted with the goal of understanding the effects of distal-tip geometry, amplitude of vibration and frequency on the onset of cavitation. Finally, the model will be validated against experimental results reported in the literature in a peripheral arterial phantom. It is envisaged that this acoustic finite element model will be capable of predicting distal-tip acoustic pressure, the onset of cavitation with the inclusion of an adequate threshold value and also in determining the extent of standing wave activity in the acoustic field.

2. METHODOLOGY

Computational models were developed using a commercially available finite element package (ANSYS©). *Fluid29* elements were used to model the acoustic fluid and all models were axisymmetric, making use of symmetrical conditions generally encountered in wire waveguide design.

The model also required the inclusion of an infinite absorbing boundary layer to define the outer limit of the acoustic model. This infinite acoustic boundary, using fluid elements *Fluid129*, was set up along the model boundary according to the condition that it must lie on an arc of radius greater than 0.2λ, where λ is the dominant wavelength. This condition is required for accurate solutions and is based on numerical experiments reported elsewhere [15].

The dominant wavelength is the greatest wavelength that may occur in the given model. As the same model may be used for a range of frequencies, with a number of materials, it is important to ensure that the dominant wavelength is correctly calculated. Given $\lambda = c/f$, this occurs for the minimum value of frequency (f) modelled and in fluids where with the speed of sound (c) is greatest.

For the minimum frequency of interest in ultrasound angioplasty (20 kHz) and given that the following models may contain up to two fluids i.e. blood and air, the greatest wavelength occurs in the blood with a value of approximately 79 mm. Using this dominant wavelength the location of the infinite acoustic boundary arc must be located at a distance greater than 16 mm from the structural source. An outgoing pressure wave reaching the boundary of the model is absorbed with minimal reflections back into the fluid domain. The infinite elements perform well for low as well as high frequency excitations [16].

The 2-D fluid elements that are used for acoustic modelling have four corner nodes with three degrees of freedom per node, displacements in the x and y directions and pressure, and are governed by the lossless wave equation.

The fluid-structure interface is defined where the wire waveguide distal-tip and fluid meet. The interaction of the fluid nodes and structural nodes at the fluid-structure interface is such that the pressure in the acoustic field exerts an applied force on the structural elements that produce an effective fluid load. The governing equations for both the fluid nodes and structural nodes are shown in equation 7. Figure 4 shows an example of the model geometry and mesh structure.

All models were solved for a harmonic vibratory distal-tip displacement on the fluid-structure interface (FSI). The input amplitude of vibration on the FSI specified the amplitude of vibration of the distal-tip. A frequency sweep was performed for a range of frequencies of interest. The plots of pressure dependence on amplitude and frequency were generated.

a. Model verification: mesh density analysis

Understanding the effect of the mesh density on the model's ability to resolve the pressures in the fluid field and near the distal-tip is critical in the determination of device operation and in predicting the onset of cavitation. An acoustic axisymmetric model was

created of a wire waveguide with a spherical distal-tip vibrating in a fluid, which represented blood at 22.5 kHz.

A mesh density study was performed in which the number of elements per wavelength (EPW) was increased until the predicted pressures from the model agreed closely with the analytical solution for an oscillating sphere, as outlined in equation 1.

Since the wavelength is frequency dependent, a range of frequencies and distal-tip amplitudes of vibration were modelled to verify that the models are still accurate in predicting acoustic pressures, using this EPW count, for the typical parameters encountered during the clinical application of ultrasound angioplasty.

b. Acoustic pressure field versus waveguide parameters

Using the verified model with the appropriate mesh density, as determined from the above methodology, a number of distal-tip geometries similar to those reported in the literature were modelled. The acoustic pressure field associated with each distal-tip design was assessed for a range of amplitudes of vibration based on those parameters commonly reported. The distal-tip geometries modelled (diagrams included in graphs) were:

i. Spherical distal-tip, used for model verification
ii. Radiused distal-tip (1 mm diameter)
iii. Flat distal-tip (1 mm and 2 mm diameter)
iv. Inverted dome distal-tip (1 mm diameter)

c. Model validation: *In vivo* model in a peripheral artery

Since neither method (FEA or analytical) accounts for the non-linear wave propagation of ultrasound, a validation of the model was particularly relevant. To validate the linear acoustic finite element method for this application and to further understand the effect of an air interface on the acoustic pressures during ultrasonic angioplasty a model representative of Makin and Everbach's [10] experimental study using a 22.5 kHz wire waveguide device was created. This was similar to the *in vivo* scenario of an artery within a peripheral limb and takes into account the acoustic tissue-air interface typically encountered.

Where the previous finite element models above focused on single fluid fields, the validation model required other complexities such as a blood/tissue-air interface. The model incorporated fluid (blood) and air properties, geometries and frequency of operation outlined in Makin and Everbach's experiment. While the distal-tip amplitude of vibration was given for high power settings the authors did not provide low-power parameters. Based on similar equipment and set-ups it was inferred to be 10% of total output $\approx 6.5\mu m$ amplitude of vibration.

The aim of this finite element model was to examine if one could accurately predict the pressures recorded and also determine the standing wave generated in Makin's experiment using linear assumptions. This would validate the mesh density study and examine whether or not ultrasound at these frequencies and amplitudes of vibration can be described by assuming linear relationships.

3. RESULTS AND DISCUSSION

a. Model verification and mesh density analysis

The mesh density analysis results are shown in Figure 5 and Table 1. The results clearly show the effect of insufficient mesh density when trying to accurately predict the pressure amplitudes at the distal-tip of the waveguide and in the acoustic field around the waveguide.

The model was initially meshed with 20 EPW as reported by others, in similar applications, to be sufficient [17-21] and then increased until a good correlation was achieved with the pressures directly ahead of the spherical distal-tip as determined from the analytical solution. This was shown to amount to at least 140 EPW for the conditions of interest. This highlights the importance of adequate discretization of the acoustic domain to predict the maximum pressures at the wire distal-tip.

For 20 EPW, the predicted maximum pressure at the wire distal-tip was approximately 280 kPa, significantly lower than the distal-tip pressure of approximately 590 kPa given by the analytical solution. 140 EPW were required to closely predict the analytical pressures. These results highlight how significant suboptimum meshing can be, rendering models prone to errors and inaccuracies. The magnitude of the discrepancies between the analytical solution and FEA model for maximum pressures at the spherical distal-tip surface can be seen in Table 1. It also shows that a percentage difference of approximately 2.5% can be achieved when compared with the analytical solution for an element count of 140 EPW.

Since these devices are often used over a range of frequencies and distal-tip amplitudes of vibration, a number of models were created using a distal-tip amplitude of vibration of 50 µm, for a range of frequencies (20 - 50 kHz), using the 140 EPW established from previous results. The results (only two frequencies presented for clarity) are shown in Figure 6. The purpose of this was to examine the effects of frequency and distal-tip amplitude of vibration on the accuracy of the model using 140 EPW. This study also showed that 140 EPW produced pressure profiles with close agreement to the Morse analytical solution for the frequencies and distal-tip amplitudes of vibration modelled.

b. Acoustic pressure field versus wire waveguide distal-tip geometry

Using 140 EPW and an operating frequency of 23.5 kHz, the following results were achieved for the distal-tip geometries modelled:

Figure 7 shows the pressure results for the 1 mm radiused distal-tip for a range of wire waveguide distal-tip amplitudes of vibration up to 60 µm. The predicted pressures show clearly the effect that increasing distal-tip amplitude of vibration has on the waveguide performance. With the inclusion of a cavitation threshold relevant to the *in vivo* conditions, the onset of this critical event may be predicted.

It is also possible to compare the effect that distal-tip geometry has on waveguide performance. Figure 8 shows the predicted pressures for a 1 mm flat head distal-tip. For the 1 mm radiused distal-tip, the maximum pressure is approximately 300 kPa (60 µm amplitude of vibration). For the same amplitude of vibration, a 1 mm flat head produces nearly 550 kPa. The 1 mm inverted dome for the same amplitude of vibration, as shown

in Figure 9, produces nearly 1,100 kPa, an increase of close to 300% when compared to that of the 1 mm radiused wire. The effect of distal-tip size was also assessed. For flat distal-tip heads, doubling the diameter of the wire will have a proportionate effect on the pressure; with the 2 mm flat head distal-tip wire generating 1,100 kPa, as shown in Figure 10.

Of interest, also, is that the wire distal-tip geometry produces characteristic acoustic pressure decay profiles. Ideally for the purpose of ablation of the diseased material directly ahead of the wire distal-tip, it is desirable to project the maximum pressures directly ahead as opposed to latterly, where they may damage the surrounding healthy tissue. The walls of arteries may also harbour nuclei that could generate undesirable cavitation within the healthy artery wall; therefore, these pressures should be kept to a minimum.

The inverted dome results in a favourable pressure distribution, with the walls of the dome acting as a barrier to the adjacent healthy artery wall where pressures are lower. Also, this shape acts to intensify the pressure by a focal mechanism. The spherical and radiused configurations display a wide dipole-like pressure distribution in all directions, spatially '*wasting*' some of the acoustic power that could be used to cause cavitation and ablate the diseased material directly ahead. Any proposed geometry, however, is limited by surgical interventional constraints, flexibility and the risk of arterial perforation.

c. Model validation: *In vivo* model in a peripheral artery

The results from the finite element model of the experimental tests conducted by Makin and Everbach can be divided into two sections:

Firstly, the predicted distal-tip pressures showed that significant pressure amplitudes were generated in the vicinity of the distal-tip. Given a cavitation threshold of approximately 100 - 200 kPa [5, 7] it is consistent with the occurrence of cavitation. Cavitation was experimentally detected by the authors who also commented on the relationship between the distal-tip amplitude of vibration, geometry and size, and cavitation activity detected, something that the model also captures.

Secondly, the finite element model also appears to be able to predict the standing wave observed during the experiments. At low-power settings where the wire motion is more uniform in the longitudinal direction i.e. less whipping motion, the model can reasonably predict the locations of pressure minima and maxima, as shown in Figure 11. The pressure amplitude variations may be due to a number of factors including insufficient knowledge of the original experiment (frequency and amplitude of device used), damping and attenuation, experimental material properties and non-linear effects. At higher power settings the standing wave structure observed by Makin and Everbach is significantly disrupted by a reported whipping motion of the wire waveguide.

4. CONCLUSIONS

A linear acoustic fluid-structure model appears useful in the prediction of pressure profiles and cavitation during ultrasound angioplasty. The model compared favourably with the analytical solution provided an adequate mesh density was utilised. This was determined to be approximately 140 elements per wavelength for the frequencies and amplitudes of vibration modelled and often encountered during the clinical use of these devices.

The model showed the relationship between distal-tip amplitude of vibration, frequency and the pressures developed. Increasing the frequency does increase the pressure substantially; however, the intensities to cause cavitation also increase. Most devices operate in the region up to 50 kHz and the EPW count was shown to be sufficient over the range.

Unlike the analytical solution, the model was not restricted to simplified geometries. The acoustic pressure results for the range of distal-tips modelled showed that the geometries not only affected the distal-tip surface pressure but also altered the overall acoustic profile around the distal-tip, such as the decay distance etc. This may play a critical role as it can be used to alleviate lateral pressures that may adversely affect healthy arterial tissue. The inverted dome distal-tip, for example, resulted in greater pressures (when compared with other distal-tip geometries for similar conditions) that were focussed directly ahead of the distal-tip. With the inclusion of validated cavitation threshold value for tissues and blood at these frequencies the model may be able to predict regions where cavitation would occur.

The finite element model of the published experimental procedure demonstrated that a linear acoustic modelling approach may be useful in the design of wire waveguide distal-tip geometries and could be further used to predict acoustic pressure profiles in relatively complex environments with tissue-air interfaces, such as the peripheral artery as demonstrated here.

In conclusion a linear acoustic fluid-structure model appears useful in understanding how distal-tip design changes and amplitudes of vibration can affect pressure amplitudes, onset of cavitation and overall acoustic field studies, and can be an effective design tool for such devices.

Acknowledgements

This work was funded under the HEA Technology Sector Research: Strand I.

REFERENCES

1. Ng, W., Chen, W.H., Lee, P-Y, Lau, C.P., Initial experience and safety in the treatment of chronic total coronary occlusions with a new optical coherent reflectometry-guided radiofrequency ablation guidewire. *The American Journal of Cardiology,* 2003; 92: 732-734.
2. Flowcardia Inc. The crosser catheter system. *Flowcardia Inc, Press Releases. www.flowcardia.com.* 2007.
3. Shaul Atar H. L., Nagai T. and Siegel R. J. Ultrasonic thrombolysis: catheter-delivered and transcutaneous applications. *European Journal of Ultrasound,* 1999; 9: 39-54.
4. Yock P.J. and Fitzgerald P.J. Catheter-based ultrasound thrombolysis shakes, rattle and reperfuse. *Circulation,* 1997; 95:1360-1362.
5. Perkins J.P. Power ultrasonic equipment: practice and application. *Sonochemistry Symposium, Annual Chemical Congress, Warwick University,* 1986: 8-11.
6. Morse P.M. Vibration and sound, *Acoustic Society of America,* 1981; 27: 311-326.
7. Nyborg W.L. Chapter 1: Basic physics of low frequency therapeutic ultrasound, Ultrasound angioplasty. *Developments in Cardiovascular Medicine*, (Ed. by Siegel R.J.). Kluwer Academic Publishers, 1996.
8. Steffen W and Siegel R. J. Ultrasound angioplasty - A review. *Journal of Interventional Cardiology.* 1993; 6: 77-88.
9. Chikada M. An experimental study of surgical ultrasonic angioplasty: Its effect on atherosclerosis and normal arteries, *Annals of Thoracic Surgery,* 2004; 77: 243-6.
10. Makin I. R. and Everbach E. C. Measurement of pressure and assessment of cavitation for a 22.5-kHz intra-arterial angioplasty device. *J. Acoust. Soc. Am.*, 1996; 100(3): 1855-64.
11. Porges G. *Applied Acoustics*: 1977. Edward Arnold, London.
12. *Ansys Theory Reference*. Chapter 8: Acoustics. *ANSYS Documentation*, ANSYS, Inc, Canonsburg, PA 15317.
13. Gavin G. P., McGuinness G.B., Dolan F. and Hashmi M.S.J. Performance Characteristics of a Therapeutic Ultrasound Wire Waveguide. *International Journal of Mechanical Sciences*, 2007; 49 (3): 298-305.Porges G., *Applied Acoustics*: 1977. Edward Arnold, London.
14. Gavin G. P., Dolan F., Hashmi M.S.J. and Mc Guinness G.B. A coupled fluid-structure model of a therapeutic ultrasound angioplasty wire waveguide. *Journal of Medical Devices,* 2007; 1: 254-263.
15. *Fluids Analysis Guide*, Subsection 15: Acoustics. *ANSYS Documentation*. ANSYS, Inc., Canonsburg, PA 15317.
16. Khan M.S., Cai C., Hung K. C., Acoustics Field and Active Structural Acoustic Control Modelling in ANSYS, *International ANSYS Conference Proceedings*, 2002.
17. Hill R., Forsyth S. A. and Macey P. Finite element modelling of ultrasound, with reference to transducers and AE waves. *Ultrasonics* 2004; 42: 253-258.
18. Zhang C. S., Zou D. H. and Madenga V. Numerical simulation of wave propagation in grouted rock bolts and the effects of mesh density and wave

frequency. *International Journal of Rock Mechanics and Mining Sciences,* 2006; 43: 634-639.
19. Sumelka T. L.W. Limitations in applications of finite element method in acoustic numerical simulation. *Journal of Theoretical and Applied Mechanics,* 2006; 44: 849-865.
20. Lewis J.P., Gardner S. and Corp I. A 2D finite element analysis of an ultrasonic cleaning vessel: Results and comparisons. *International Journal of Modelling and Simulation,* 2007; 27: 181-185.
21. Zampolli M., Tesei A. and Jensen F.B. Finite element models for the solution of underwater acoustics problems. *COMSOL Multiphysics User's Conference,* Stockholm, 2005.

Appendix of Tables

EPW	20	40	60	80	100	120	140	300
FEA. Max pressure at distal-tip (Pa)	269,490	402,210	471,100	509,540	532,560	547,220	587,040	589,510
% Difference from analytical solution	53	29.7	17.7	11	7	4.5	-2.4	-2.9

Table 1: Percentage difference of maximum pressure at distal-tip versus maximum pressure calculated by analytical solution (Morse [6]) for a range of EPW modelled.

Figures

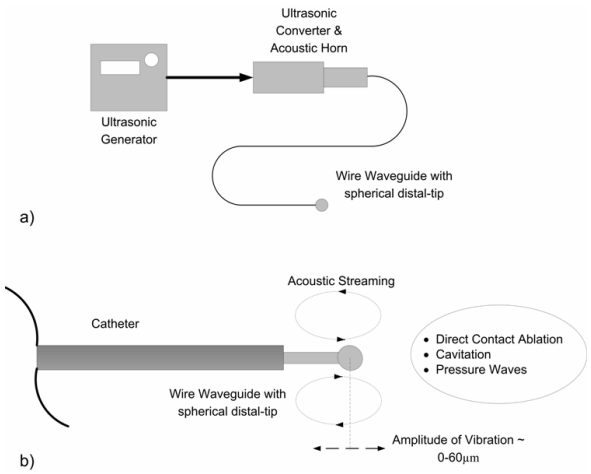

Fig 1

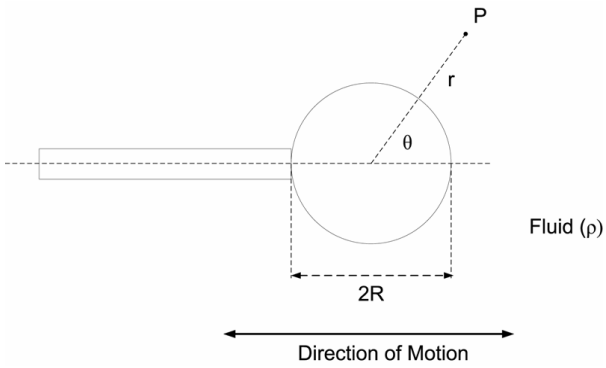

Fig 2

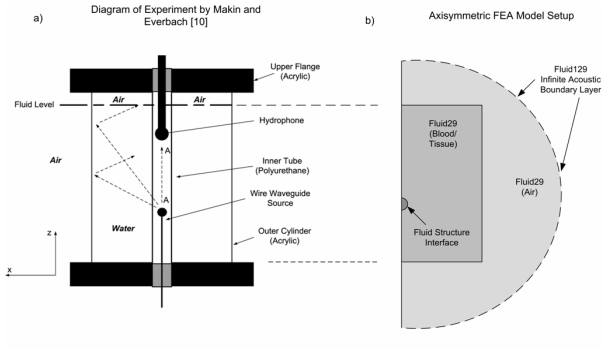

Fig 3

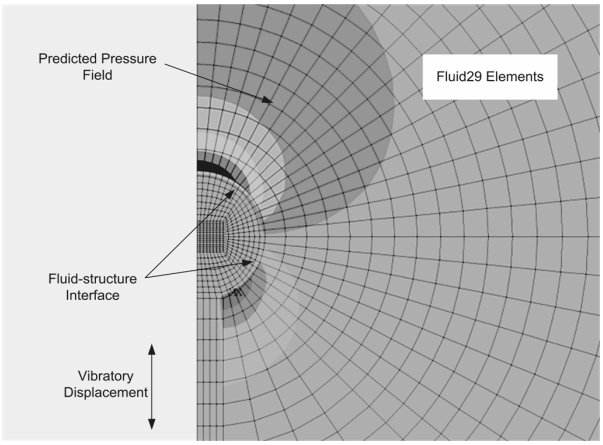

Fig 4

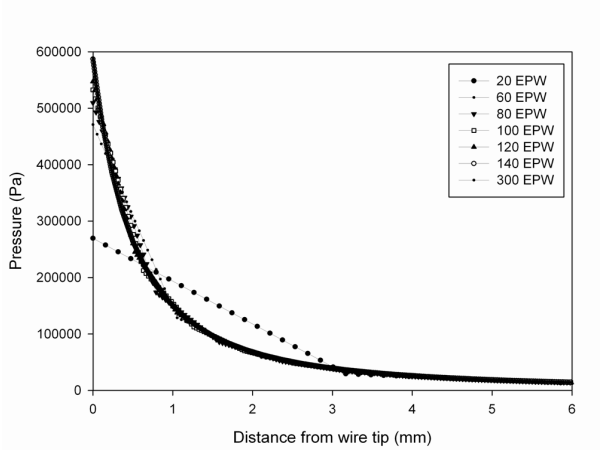

Fig 5

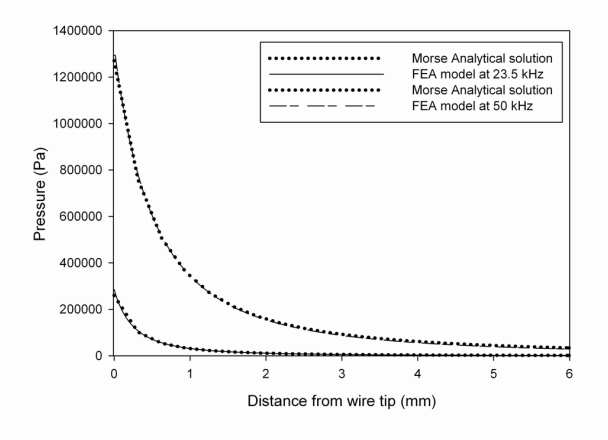

Fig 6

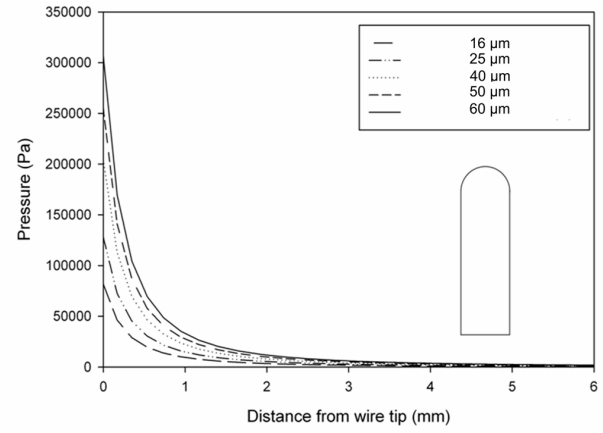

Fig 7

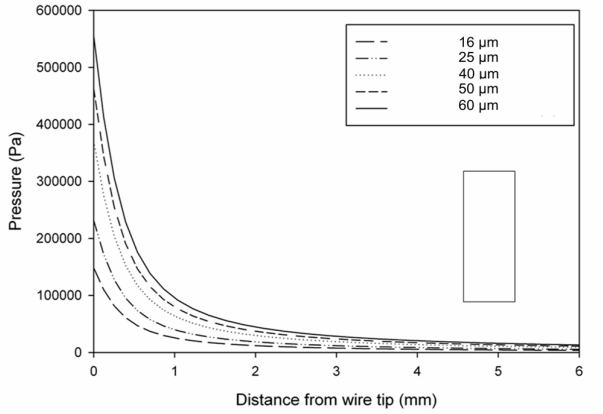

Fig 8

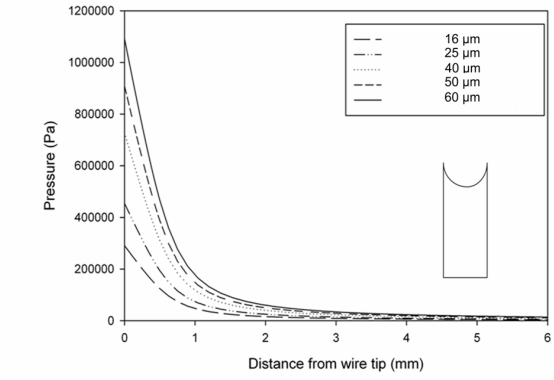

Fig 9

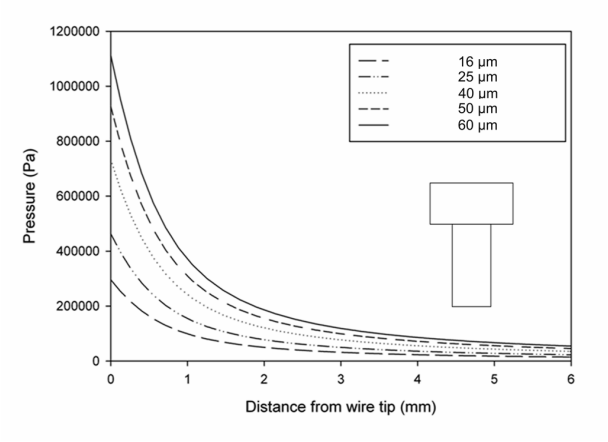
1200000
1000000
800000
600000
400000
200000
0
Pressure (Pa)
0
1
2
3
4
5
6
Distance from wire tip (mm)
16 µm
25 µm
40 µm
50 µm
60 µm

Fig 10

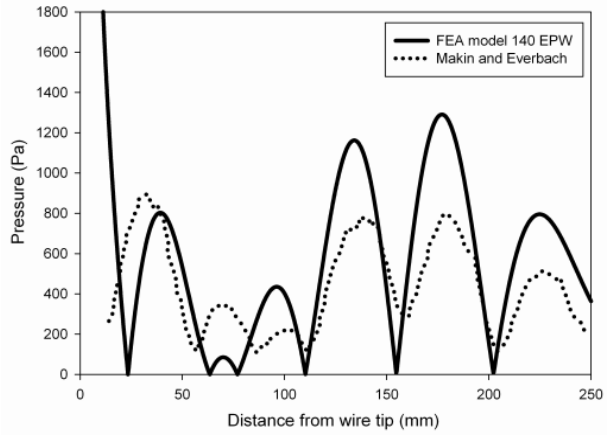
1800
1600
1400
1200
1000
800
600
400
200
0
Pressure (Pa)
0
50
100
150
200
250
Distance from wire tip (mm)
FEA model 140 EPW
Makin and Everbach

Fig 11